An Overview of Recent Developments in Microring Resonator Based Photonic Circuits

Otto Schwelb

Abstract – **Microring and microdisk resonators are used in photonic circuits to perform filter functions, serve as band-limited mirrors in lasers, compensate for dispersion and group delay distortion, are used in multiplexers in telecommunication systems, and a number of other applications such as medical instrumentation, biosensing, interferometry, to name a few. This paper outlines some challenges and solutions in this relatively new and prolific discipline.**

Keywords – **Ring resonator, Photonic circuit, Add/drop multiplexer, Optical filter, High-*Q* optical resonator.**

I. Introduction

Photonic filters and circuits performing filter functions require resonant elements. These microresonators are most often ring or disk resonators fabricated using integrated circuit technology. The size of these resonators is in the order of tens or hundreds of wavelengths, the smaller the size and the smaller the bending radii the more critical become radiation losses and fabrication tolerances. Due to their small size and thanks to significant advances in fabrication technology, high density packing of these resonators can now be realized to support VLSI photonics.

Unlike in microwave resonators where metallic boundaries exist to contain the electromagnetic field, in the optical domain one relies on the refractive index contrast to prevent leakage. This requires that careful attention be paid to the proximity and smoothness of boundary surfaces. As in microwave filter structures built with reentrant cavities, optical filters using ring resonators, or grating assisted Fabry-Pérot resonators, have a comb spectrum where the passband reappears periodically, separated by the so-called free spectral range (FSR). In multichannel communication or sensing the spectral width of the FSR is important, because within its range must fit all the passbands of the other channels of the system. The extension of the FSR to accommodate all channels is therefore one of the critical design issues of multiring resonator based photonic devices.

Another critical issue, common in filter design, is the roll-off or shape factor that defines the transition region between passband and stopband. It is well known that an increase in filter order leads to an increase in selectivity and that Butterworth (maximally flat) and Chebyshev (equal ripple) design principles are available in optical filter design, much as for microwave filters, to shape the passband. Since, however, optical resonators are coupled by the overlap of the evanescent tail of their field, construction of multiring optical filters is a more difficult process.

Otto Schwelb is with the Department of Electrical and Computer Engineering, Concordia University, Montréal, QC Canada, H3G 1M8, E-mail: otto@ece.concordia.ca

The range of applications of multiring based photonic circuits is extensive. In addition to communication filters they are used as add/drop multiplexers, sensors, mirrors, interferometers, modulators and in numerous industrial, medical and aeronautical applications. This paper focuses on functions and implementations, on analysis and design, leaving the extensive area of fabrication technology untouched. We shall begin with enumerating some of the analytical methods used in photonic circuit design, followed by a discussion of challenges, solutions and modern developments in this relatively young discipline.

II. Analytical Methods

The basic components of photonic circuits are the proximity coupler, the ring resonator, the grating, the multimode interference (MMI) coupler and the arrayed waveguide grating (AWG). Of these only the first two play an explicit role in our present discussion. The coupler consists of two waveguides in close proximity, has four ports and its function is to transfer energy from one waveguide to the other by exploiting the overlap of the evanescent tails of the optical fields of the guides [1]. For weak interactions, the coupling is the stronger the closer are the guides and the longer the region of interaction. Since the field outside the waveguide decays exponentially the separation must be a fraction of the wavelength. Although the interaction is distributed over a finite length, for analytical and numerical purposes proximity couplers are usually treated as lumped element devices, i.e., the interaction is assumed to take place in a point. A schematic representation of a coupler is shown in Fig. 1, indicating alternative pairs of connections, a_i and b_i are incoming and outgoing waves, respectively [2].

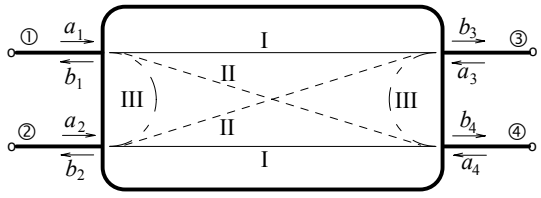

Fig. 1. Generalized lumped element 2×2 coupler. The paths I, II and III depict either direct or coupled connection between ports.

An ideal lumped element coupler has two axes of symmetry: it is both bilaterally (vertical symmetry axis) and transversally (horizontal symmetry axis) symmetric. A direct connection is defined by $\sqrt{(1-K)}$ while a coupled connection is defined by $j\sqrt{K}$, where K is the power coupling coefficient. Note that there is a $\pi/2$ phase difference between direct and coupled connections and that the total power, the sum of the magnitudes squared, is conserved. Coupler loss is admitted by

the loss factor $a = \sqrt{(1-\gamma)}$, not to be confused with the incoming wave amplitudes a_i, and γ is the fractional loss.

Ring resonators [3], [4] are defined by their average perimeter length L and by the effective refractive index of the guide n_e. The product of these numbers is the so-called optical length of the resonator. Ring resonators are also characterized by their mode number $N = Ln_e/\lambda_0$, where λ_0 is the design wavelength and by the time delay of a round trip: $\tau_0 = Ln_e/c$. Note that ring resonators need not be circular; they often have racetrack or other shapes. Critical is the bending radius which determines radiation loss. Since resonances occur whenever N is an integer the spectrum of resonances displays a comb structure. The distance between consecutive resonances is the free spectral range (FSR). The width of the FSR plays a key role in multichannel communication. It must be sufficiently wide to accommodate all channels, and it must be free of spurious signals that could interfere with them (see extending the FSR in section IV).

The most elementary but also the most cumbersome analytical method to investigate the operation of a multiring photonic circuit is to write out explicitly the node and loop equations, and extract from them the complex output wave amplitudes normalized to the input amplitude. In essence this method provides the all-important scattering coefficients of the device from which transfer intensity, phase, group delay and dispersion characteristics can be computed [5].

A transfer matrix based method has been used to obtain the characteristics of all types of photonic circuits since 1998 [2]. The gist of this method is the rearrangement of the photonic circuit into a feedback assisted four-port, the scattering matrix of which can be expressed in closed form. The four-port itself is a cascaded set of four-ports whose overall transfer matrix is evaluated by classical matrix multiplication. It turns out that by using the concept of the generalized lumped element coupler [2], virtually all 2-D photonic circuit topologies are amenable to the analytic treatment described there. A narrow-band double-ring mirror and its feedback assisted cascaded chain equivalent, shown in Fig. 2, illustrates the method.

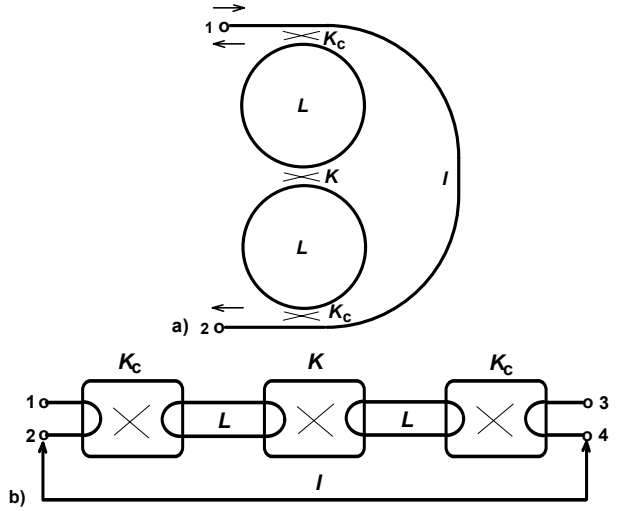

Fig. 2. Double-ring mirror device and its schematic representation.

Another analytic method applicable to series-, or direct-coupled microring circuits is the so-called iterative method illustrated in Fig. 3 [6]. The effect of the 1st ring is embedded into the second, their combined effect embedded into the third, and so on, until the effect of the entire chain is manifest in the transmission coefficient of the main bus waveguide. Analytically this is expressed by

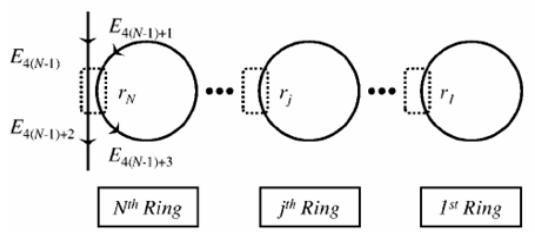

Fig. 3. Application of the iterative method to direct-coupled rings.

$$t_j = \frac{c_j - \sigma_j t_{j-1} e^{-j\beta L_j}}{1 - \sigma_j c_j t_{j-1} e^{-j\beta L_j}},\ c_j = \sqrt{1-K_j},\ \sigma_j = e^{-\alpha L_j} \qquad (1)$$

where t_j is the transmission factor embedded into the j-th ring, caused by the presence of the $(j-1)$-th.

To treat a long chain of cascaded four-ports Bloch-wave analysis, well known in microwave periodic filter and grating design, has been proposed [7]. Two examples are shown below in Fig. 4; in a) a so-called coupled-resonator optical waveguide (CROW) delay line [8] and in b) a parallel-coupled multiring filter [9].

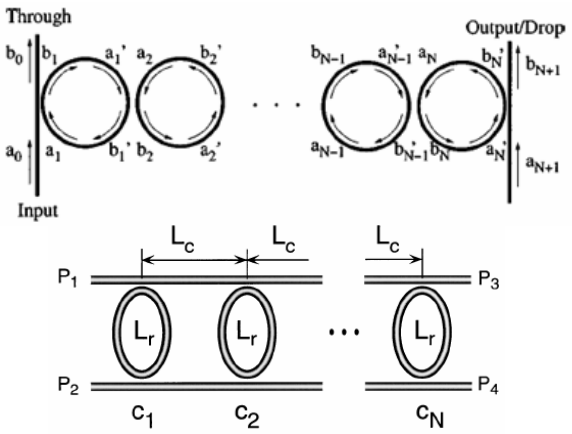

Fig. 4. a) Cascaded resonant optical waveguide (CROW), b) parallel-coupled multiring filter.

We mention one more graphical/analytical approach to treat an optical circuit, namely the signal flow graph, or Mason's method [10]. As long as the complexity of the circuit is moderate and waves circulate in the rings only in one direction, the signal flow graphs are easy to handle. However, complex circuits and/or counter-propagating waves in the rings render this method quite cumbersome. Furthermore, group delay and dispersion characteristics cannot be directly extracted from flow graphs.

The methods so far enumerated analyze the device as a circuit. More fundamental approaches consider the electromagnetic field within the integrated structure and solve the appropriate Maxwell's equations to various degrees of approximation. Extensive recent investigations on microcavities and periodic structures under the umbrella organizations *European Cooperation in the field of Scientific*

and Technical Research (*COST268*) and *Next Generation Active Integrated Optical Subsystems* (*NAIS*) produced important results regarding radiation from bent waveguides, computation of the coupling between a channel waveguide and microdisk, resonance frequency shift due to self coupling, etc. [11]. Some of these computations use the full vectorial formulation of the field, some use the coupled mode approximation, while others use the Finite Difference Time Domain (FDTD) method [12]. Fig. 5 illustrates, for example, the 1μm wavelength TE_1 whispering gallery mode of a 8μm diameter disk, obtained using bend-mode solutions of the Maxwell equations, and the geometry of a vertically coupled add/drop multiplexer. Analytical solutions were compared with those obtained by the FDTD method and showed very good agreement.

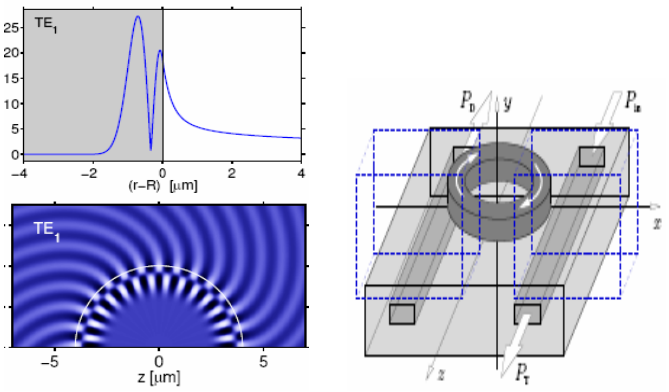

Fig. 5. TE_1 whispering gallery mode of a r = 4μm microdisk resonator and 3-D geometry of a vertically coupled add/drop filter.

III. FILTER STRUCTURES

The simplest filter using a ring resonator is an all-pass filter consisting of a ring resonator coupled to a waveguide (see Fig. 6). The filter has only two ports and if there are no discontinuities (inclusions, surface defects) in the ring it does not reflect, therefore the energy that is not absorbed in the ring must exit at the output. In the absence of loss the output intensity is equal to the input intensity. When the ring is lossy a relatively large amount of power is lost at resonance creating a notch in the transmission characteristics. The phase characteristics shown as a function of coupling strength and detuning from resonance in Fig. 7, is strongly influenced by the relationship between the loss coefficient and the coupling coefficient [4]. When $K < K_{crit} = 1 - \exp(-2\alpha L)$ the phase characteristics is anomalous, otherwise it is normal.

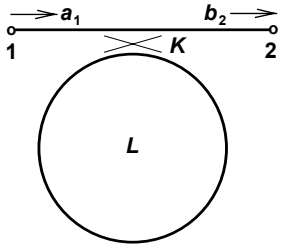

Fig. 6. Single-ring notch filter.

One of the most often used filters is the add/drop or channel dropping multiplexer. The simplest configurations are shown graphically in Fig. 8; a) and b) single-ring multiplexer, c) and d) series-coupled (or direct-coupled) double ring multiplexer, e) parallel-coupled single-ring multiplexer. The arrows indicate signal flow, coupling occurs where guides are in close proximity, and the replicated configurations of b) and d) are especially suited for dense photonic integration. The coupling between the rings, or between ring and bus guide can be lateral or vertical. The former places the coupled guides on the same plane beside each other, so the index contrast between core and cladding is restricted to small values. The latter, illustrated in Fig. 5, places ring and waveguide on different planes allowing for large index contrast and significant diameter reduction without radiation penalty.

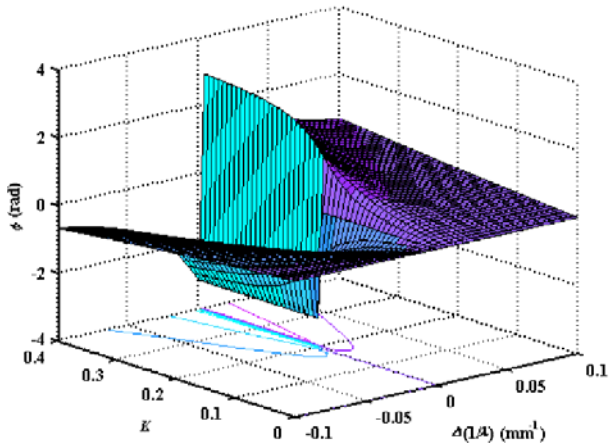

Fig. 7. Transmission phase of a ring resonator (Fig. 6) as a function of K and detuning. The loss/turn is 0.942dB. Above the critical coupling, $K_r = 0.195$, the phase characteristic changes from anomalous to normal.

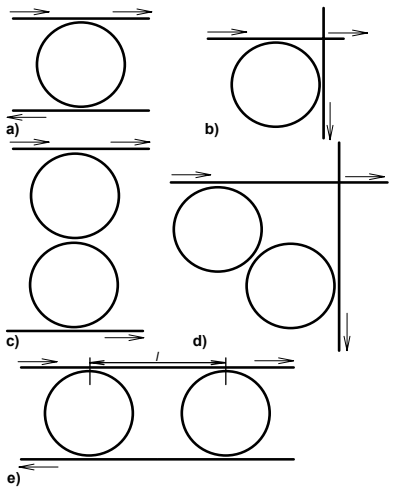

Fig. 8. Single-ring and double-ring, series-coupled and parallel-coupled add/drop multiplexer configurations.

Computed transmission and group delay characteristics of lossless direct-coupled Chebyshev (equiripple) filters of increasing order are plotted in Figs. 9 and 10 [13]. These filters have the same architecture as Fig. 4a), they are symmetric in the sense that the coupling coefficient (K_i) as

well as the perimeter length (L_i) distribution is symmetric and demonstrate the increasing roll-off steepness and increasing peak delay as the filter order increases. The synthesis procedure for this as well as for the Butterworth (maximally flat) filters follows the well known microwave filter design.

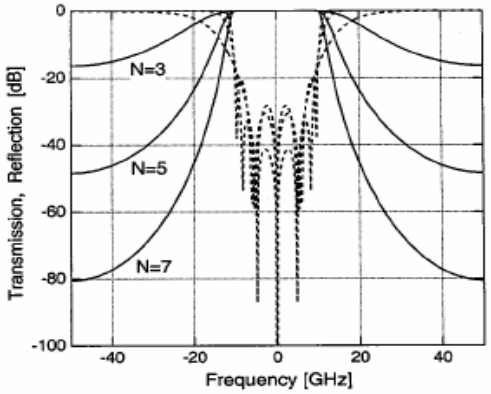

Fig. 9. Drop-port (solid) and through-port (dotted) characteristics of $N = 3$, 5 and 7 ring direct coupled Chebyshev filters, $BW = 20$GHz, $FSR = 100$GHz [13].

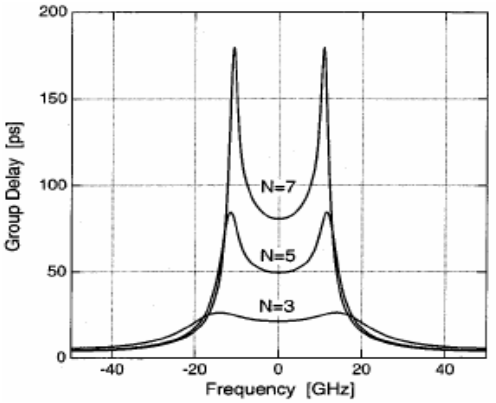

Fig. 10. Group delay characteristic of the Chebyshev filters of Fig. 9.

When the distance between adjacent rings l in Fig. 8e) is chosen appropriately to exploit the constructive interference between the two paths to the output, i.e., when the filter is phase matched, the filter provides a very convenient stopband characteristic featuring large, constant suppression shown in Fig. 11 [14]. The dotted curves of the figure also show the drop-port transmission as l deviates from optimum. The length can be adjusted by thermooptic or electrooptic means.

The improvement obtained from reducing coupling strength is demonstrated in Fig. 12, showing the drop-port and through-port characteristics of parallel-coupled triple-ring chains for three coupling coefficient combinations. Here the mode number of the rings is $N = 100$ and $2l = 100.5\lambda_0/n_e$. More complex configurations have also been proposed to improve the 1dB/10dB shape factor of parallel-coupled, phase-matched filter chains [15].

IV. Vernier Design

In order to increase the FSR of the filter to accommodate a large number of channels, the option that avoids a drastic reduction of the ring radius calls for it to be changed fractionally according to the expression

$$m_1 FSR_1 = m_2 FSR_2 = FSR \tag{2}$$

where m_1 and m_2 are integers, FSR_1 and FSR_2 refer to the two rings of the device and FSR is the resultant extended free spectral range. Simple arithmetic yields

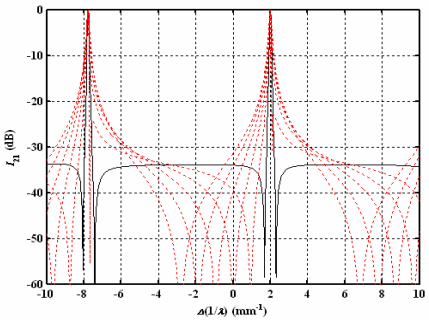

Fig. 11. Drop-port transmission of the phase-matched, double-ring filter of Fig. 8e). Dotted plots show the effect of deviation from exact phase matching.

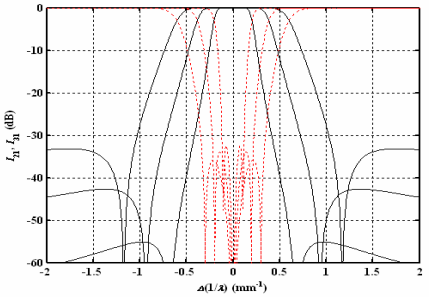

Fig. 12. Drop-port (solid) and through-port (dotted) characteristics of parallel-coupled, phase-matched triple-ring filters. Narrow band: $K_1 = 0.2$, $K_2 = 0.0116$, medium band: $K_1 = 0.35$, $K_2 = 0.041$, wide band: $K_1 = 0.5$, $K_2 = 0.0985$.

$$FSR = \frac{c(m_1 - m_2)}{n_g (L_1 - L_2)} \tag{3}$$

where n_g is the group index. These expressions indicate that by proper selection of m_1 and m_2 arbitrarily large extension ratios can theoretically be obtained, however the suppression of interstitial modes in the stopband, which must be at least 20-25dB, imposes a limit [16]. A double-ring Vernier filter together with its drop-port characteristics is shown in Fig. 13, indicating that the spurious modes adjacent to the passband at $f_0 \pm FSR_{1,2}$ are not sufficiently suppressed [17].

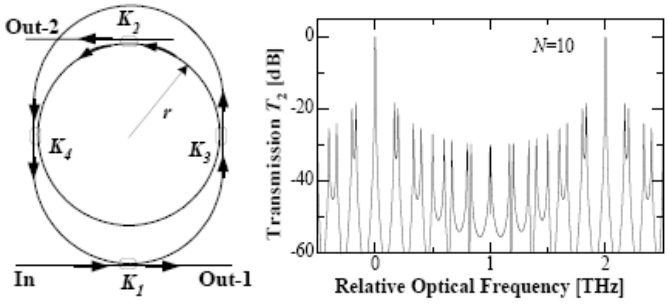

Fig. 13. A double-ring Vernier filter [17] and its drop-port characteristics $K_1 = K_2 = 10^{-6}$, $K_3 = K_4 = 10^{-4}$, $m_1 = 10$.

A universal curve [16] has been obtained for direct-coupled double- and triple-ring multiplexers that can be used to

determine the minimum percentile perimeter length reduction to ensure a set level of suppression of the most critical interstitial signals at $f_0 \pm FSR_1$. This universal curve, valid for $K_1 = 0.01$, shown in Fig. 14, can be applied to both double- and triple-ring filters. When the ring-to-waveguide coupling is different from 0.01 the expression

$$Supp_{new}^{[dB]} = Supp_{old}^{[dB]} + 20\lg\left(\frac{K_{1,new}}{K_{1,old}}\right) \quad (4)$$

can be used to determine the new level of suppression.

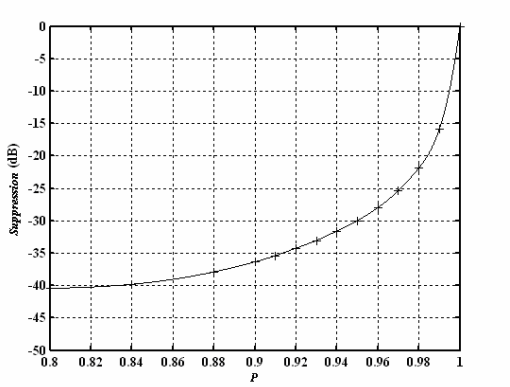

Fig. 14. Suppression of the most critical interstitial resonance at $f_0 \pm FSR_1$ in lossless double-ring and asymmetrical triple-ring filters as a function of percentile size reduction, using $K_1 = 0.01$ and $K_2 = 1.533\times10^{-5}$. Use (4) to compute the suppression for other K_1 values.

V. Mirrors and Reflectors

Beginning with the fiber loop reflector [18], one of earliest fiber optic device consisting of a 3dB coupler terminated by a fiber loop, several microring resonator based devices have been reported for use as band limited reflectors and laser mirrors [19-24]. Two of these devices are shown in Fig. 15. They have two ports, port 1 is the input port which reflects in a narrow band of frequencies (the passband) all the input intensity except the fraction that is absorbed by mirror losses, and port 2 where the input signal that falls outside the passband exits. Denoting the coupling coefficient(s) between the mirror and the bus waveguide by K_c, the mirrors are optimized in the sense that for a given K_c the internal couplings are chosen to provide a sufficient suppression level, say –25dB, for the throughput intensity in the passband.

A typical optimized reflection (I_{11}) and transmission (I_{21}) characteristic of a lossless mirror depicted in Fig. 15a) is shown in Fig. 16. The design wavelength is $\lambda_0 = 1.55\mu m$, $n_e = 1.5$, $L = 0.517$mm ($N = 500$), $K_c = 0.3$ and $K = K_{opt} = 0.178$. The abscissa represents detuning from resonance (f_0); to obtain its value in Hz multiply by the velocity of light in vacuum in mm/s. In the optimization process we selected a K value that provided an insertion loss (IL) of approximately –27dB at f_0. Fig. 17 plots the dependence of K_{opt} on K_c, at $IL = -27$dB, for a lossless mirror. Optimization does not depend on L, but the BW is inversely proportional to it. Fig. 17 also plots the BW at $IL = -15$dB, for $L = 0.207$mm ($N = 200$). To obtain the corresponding BW for e.g., $N = 500$ divide the BW values of Fig. 17 by the perimeter ratio: 2.5. As K_c is increased the rejection diminishes, $K_c \leq 0.25$ will ensure a maximum rejection of more than 25dB at the centre of the stopband.

The reflection coefficient of the mirror is diminished by the amount of power lost (due to absorption, radiation, etc.) in the rings. Reflection coefficients of four mirror configurations as a function of K_c using $N = 200$ and α =2dB/cm appear in [23].

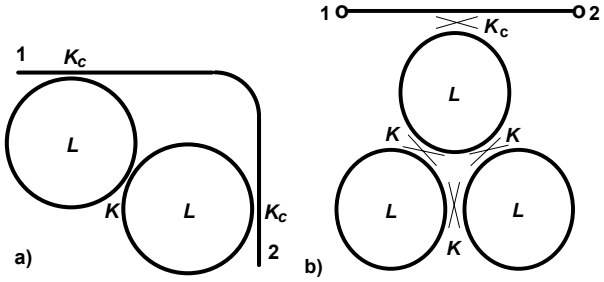

Fig. 15. A double- [23] and a triple-ring [20] mirror structure.

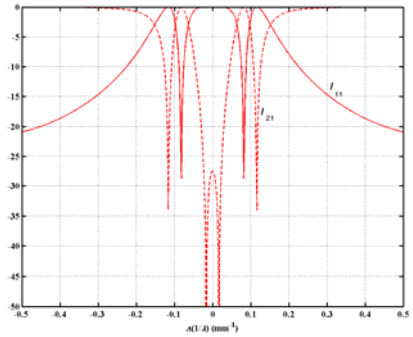

Fig. 16. Reflection (solid) and transmission (dotted) characteristics of the double-ring mirror of Fig. 15a), parameters are given in the text.

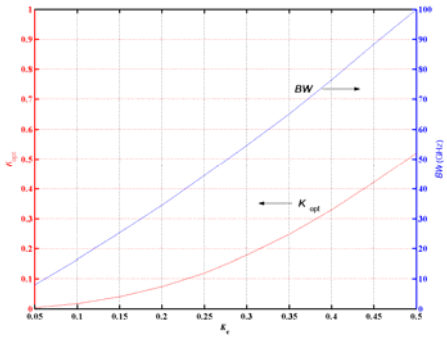

Fig. 17. Dependence of K_{opt} and BW on K_c in Fig. 15a) ($N = 200$). The bandwidth is inversely proportional to L. $K_c \leq 0.25$ ensures larger than 25dB rejection at the centre of the stopband.

VI. Composites and Phase Engineering

With the advent of high precision fabrication technology and new materials, offering high index contrast and low material dispersion, construction of compact, high density multiring devices and a new discipline, appropriately named 'phase engineering' is emerging. In this regard the first to mention are concatenated single- and double-microring waveguides, illustrated in Figs. 18 to 20.

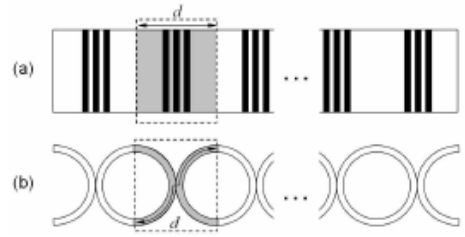

Fig. 18. Coupled resonator optical waveguide (CROW) shown as cascaded gratings (a) and direct-coupled microrings (b) [25].

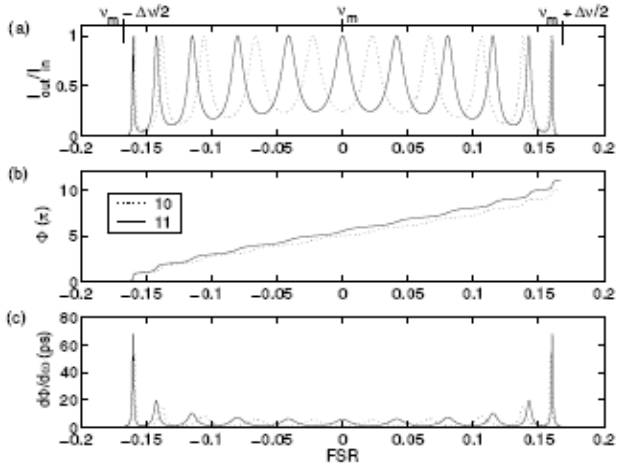

Fig. 19. Transmission a), phase b) and group delay c) response of the 10 and 11 element CROW shown in Fig. 18.

Considering Fig. 20 observe that the single channel SCISSOR (top) and the twisted double channel SCISSOR (bottom) waveguides support co-directional wave propagation. As a result these waveguides have no bandgap and their group delay remains finite. In contrast the double channel SCISSOR waveguide supports contra-directional wave propagation, there are forbidden gaps in the Bloch diagram and the group index has poles at the band edges. Two qualitatively different type of bandgaps occur. For spectral components satisfying the Bragg condition: $\lambda = 2n_eL/m_B$, where L is the spacing between the rings, the bandgap is direct and results from distributed Bragg reflection. For spectral components satisfying ring resonance: $\lambda = 2\pi n_eR/m_R$, the bandgap is indirect and results from strong resonator-mediated backcoupling. The numbers that appear in this diagram are those of m_B and m_R, respectively.

A series-parallel coupled microring stopband filter has been reported providing characteristics very similar to a long Bragg grating [27]. The transmission and group delay responses shown in Fig. 22 for filters built with $N + 2$ rings have the same features as shallow Bragg gratings with large $N_G\Delta n/n$ numbers, where $\Delta n/n$ is the relative index difference. The coupling coefficients between the rings were 7×10^{-4}, those between the rings and the buss-bar 0.214 and the ring circumferences at the design frequency were 150 wavelengths. The extremely high peaks of the band edge group delay speaks of reduced speed of wave propagation ('slow light') in this frequency region.

Phase engineering recently has produced more audacious microring configurations, two of which are introduced below. The first is a coupled ring-enhanced Mach-Zehnder interferometer [28], depicted in Fig. 23. Coupling occurs between rings within a column but not between columns. Fig. 24 plots the transmission amplitude (top), the effective phase (middle) and the bar output (bottom) of a 6 × 6 ring device with $K = 0.36$ power coupling coefficients. The second is a mutually coupled matrix of microrings, shown in Fig. 25, where the first and last rings are coupled to the input/output waveguides. Any one ring can be coupled to a maximum of four adjoining units. In [29] a synthesis procedure for elliptic filters of this configuration is presented. Fig. 26 plots the S_{11} and S_{21} parameters of a 6th order prototype filter. The filter is designed to have 0.05dB passband ripple and 40dB stopband rejection. The inset shows the computed passband response.

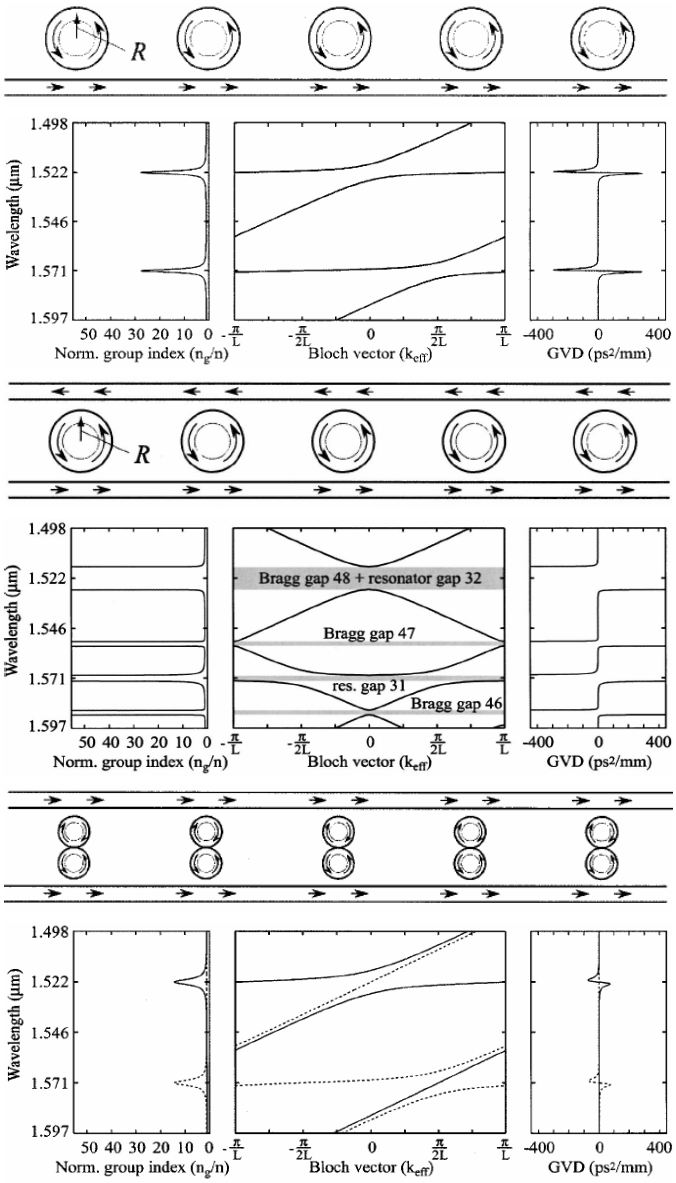

Fig. 20. Three SCISSOR waveguides and their normalized group index, effective propagation vector and group velocity dispersion response as a function of wavelength [26].

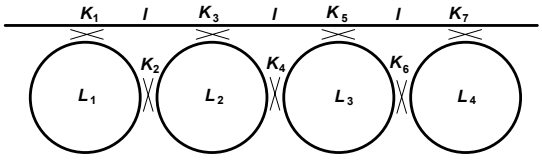

Fig. 21. Mutually-coupled microring stopband filter.

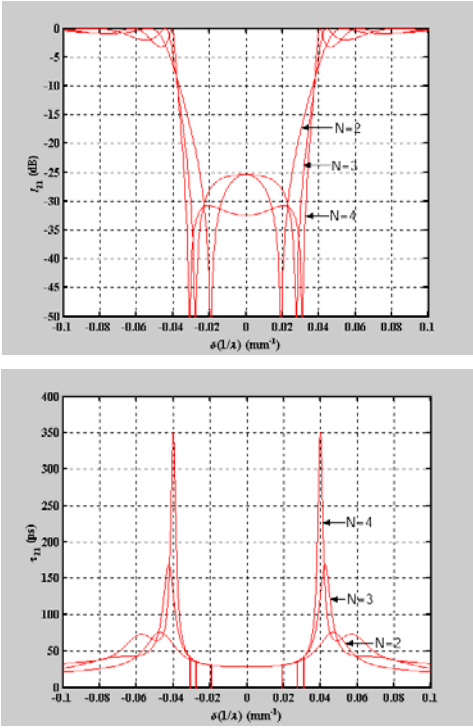

Fig. 22. Transmission (top) and group delay (bottom) responses of the mutually-coupled filter of Fig. 21 with $N + 2$ rings.

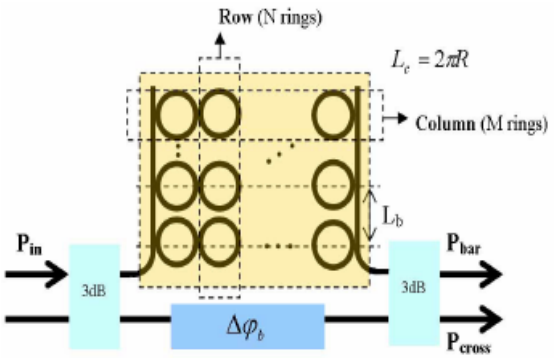

Fig. 23. Coupled ring-enhanced Mach-Zehnder interferometer. Coupling occurs between rings within the column, but not between columns [28].

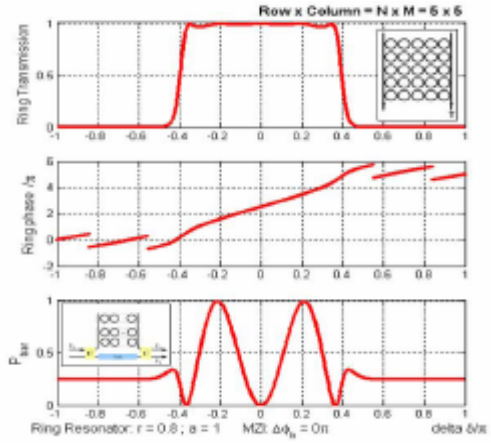

Fig. 24. Transmission amplitude (top), effective phase (middle) and bar output (bottom) of the interferometer in Fig. 23 [28].

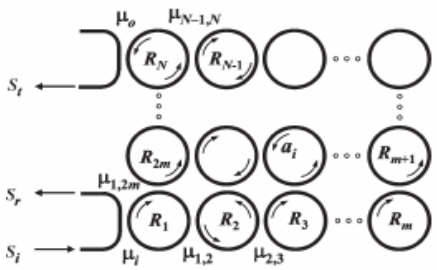

Fig. 25. 2-D array of N mutually coupled resonators where the first and last rings are coupled to the output waveguides [29].

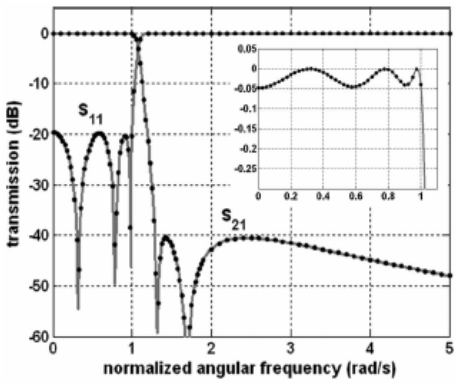

Fig. 26. S_{11} and S_{21} parameters of a 6th order prototype filter with 0.05dB passband ripple and 40dB stopband rejection. The inset shows the computed passband response [29].

Further composite devices, which we can only briefly mention in this review, are the vertically stacked multiring resonator [30] and the coiled optical resonator [31], shown below in Figs. 27 and 28, respectively.

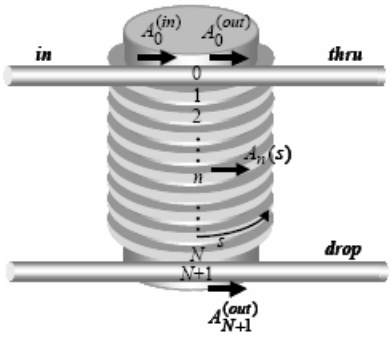

Fig. 27. The vertically stacked multiring resonator [30].

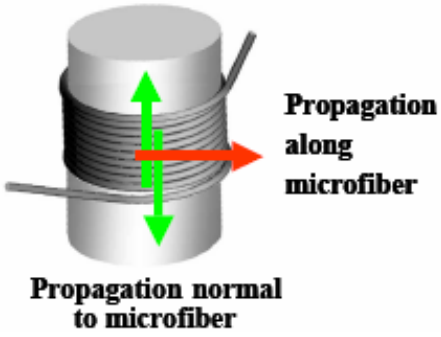

Fig. 28. The coiled optical resonator (COR) [31].

In closing we would like to mention that thanks to improved fabrication technology resonator loaded *Q* factors in recent years have reached 139,000 [32, 33] and that these huge values have been reached as the ring radius continues to decrease.

VII. CONCLUSIONS

An overview of challenges and some solutions in the field of modern photonic microresonator devices used in telecommunications and sensing has been presented. Emphasis was placed on experimental and simulated performance characteristics, while technological and fabrication aspects were left untreated. Important recent developments in microresonator devices associated with active components, electrooptic and themooptic control, and the vast area of nonlinear applications were also considered outside the scope of this review.

ACKNOWLEDGEMENT

The support of the Natural Sciences and Engineering Research Council of Canada is acknowledged.

REFERENCES

[1] H.A. Haus, *Waves and Fields in Optoelectronics,* Englewood Cliffs, Prentice-Hall, Inc., 1984, sec. 7.6.

[2] O. Schwelb, "Generalized analysis for a class of linear interferometric networks. Part I: Analysis," *IEEE Trans. Microwave Theory Tech.,* vol. 46, no. 10, pp. 1399-1408, 1998.

[3] D.H. Geuzebroek and A. Driessen, "Ring-resonator-based wavelength filters" in: *Wavelength Filters in Fibre Optics*, Springer series in optical sciences 123/2006. Springer Verlag, Berlin/Heidelberg, pp. 341-379.

[4] O. Schwelb, "Transmission, group delay and dispersion in single-ring optical resonators and add/drop filters - A tutorial overview," *J. Lightw. Technol.,* vol. 22, no. 5, pp. 1380-1394, 2004.

[5] S.J. Emelett and R.A. Soref, "Synthesis of dual-microring-resonator cross-connect filters," *Optics Express,* vol. 13, no. 12, pp. 4439-4456, 2005.

[6] D.D. Smith, et al., "Coupled-resonator-induced transparency," *Phys. Rev. A,* vol. 69, 06384 2004.

[7] M. Cherchi, "Bloch analysis of finite periodic microring chains," *Appl. Phys. B.* vol. 80, pp. 109-113, 2005.

[8] J.K.S. Poon, J. Scheuer, Y. Xu and A. Yariv, "Designing coupled-resonator optical waveguide delay lines," *J. Opt. Soc. Am. B,* vol. 21, no. 9, pp. 1665-1673, 2004.

[9] A. Melloni, "Synthesis of a parallel-coupled ring-resonator filter," *Opt. Lett.,* vol. 26, no. 12, pp. 917-919, 2001.

[10] I.S. Hidayat, et al, "Application of transfer matrix method with signal flow-chart to analyze optical multi-path ring-resonator," *Mem. Fac. Eng. Okayama Univ.,* vol. 36, no. 2, pp. 73-82, 2002.

[11] F. Michelotti, A. Driessen and M. Bertolotti, eds. *Microresonators as Building Blocks for VLSI Photonics,* AIP Conference Proceedings, vol. 709, 2004.

[12] S. C. Hagness, D. Rafizadeh, S. T. Ho and A. Taflove, "FDTD microcavity simulations: design and experimental realization of waveguide-coupled single-mode ring and whispering-gallery-mode disk resonators," *J. Lightw. Technol.,* vol. 15, no. 11, pp. 2154-2165, 1997.

[13] A. Melloni and M. Martinelli, "Synthesis of direct-coupled-resonators bandpass filters," *J. Lightw. Technol.,* vol. 20, no. 2, pp. 296-303, 2002.

[14] O. Schwelb, and I. Frigyes, "A design for a high finesse parallel-coupled microring resonator filter," *Microwave Opt. Technol. Lett.,* vol. 38, no. 2, pp. 125-129, 2003.

[15] O. Schwelb, and I. Frigyes, "Parallel-coupled phase-matched multiring optical filters," *Microwave Opt. Technol. Lett.,* vol. 44, no. 6, pp. 536-540, 2005.

[16] O. Schwelb, "The nature of spurious mode suppression in extended FSR microring multiplexers," *Opt. Commun.,* vol. 271, no. 2, pp. 424-429, 2007.

[17] I.S. Hidayat, et al, "Application of transfer matrix method with signal flow-chart to analyze optical multi-path ring-resonator," *Mem. Fac. Eng. Okayama Univ.,* vol. 36, no. 2, pp. 73-82, 2002.

[18] D.B. Mortimore, "Fiber loop reflectors," *J. Lightw. Technol.,* vol. 6, no. 7, pp. 1217-1224, 1988.

[19] B. Liu, A. Shakouri and J.E. Bowers, "Wide tunable double ring resonator coupled lasers," *IEEE Photon. Technol. Lett.,* vol. 14, no. 5, pp. 600-602, 2002.

[20] J.K.S. Poon, J. Scheuer and A. Yariv, "Wavelength-selective reflector based on a circular array of coupled microring resonators," *IEEE Photon. Technol. Lett.,* vol. 16, no. 5, pp. 1331-1333, 2004.

[21] I. Chremmos and N. Uzunoglu, "Reflective properties of double-ring resonator system coupled to a waveguide," *IEEE Photon. Technol. Lett.,* vol. 17, no. 10, pp. 2110-2112, 2005.

[22] Y. Chung, D.-G. Kim and N. Dagli, "Widely tunable coupled-ring reflector laser diode," *IEEE Photon. Technol. Lett.,* vol. 17, no. 9, pp. 1773-1775, 2005.

[23] O. Schwelb, "Band-limited optical mirrors based on ring resonators: analysis and design," *J. Lightw. Technol.,* vol. 23, no. 11, pp. 3931-3946, 2005.

[24] G.T. Paloczi, J. Scheuer and A. Yariv, "Compact microring-based wavelength-selective in-line optical reflector," *IEEE Photon. Technol. Lett.,* vol. 17, no. 2, pp. 390-392, 2005.

[25] Y. Chen and S. Blair, "Nonlinearity enhancement in finite coupled-resonator slow-light waveguide," *Optics Express,* vol. 12, no. 15, pp. 3353-3366, 2004.

[26] J.E. Heebner, et al., "Distributed and localized feedback in microresonator sequences for linear and nonlinear optics," *J. Opt. Soc. Am. B.* vol. 21, no. 10, pp. 1818-1832, 2004.

[27] O. Schwelb, "Some novel photonic bandpass and bandstop filters," *Proc. ISMOT 2001*, Montreal, Canada, June 19-23, pp. 141-144, paper # 105.

[28] S. Darmawan, Y.M. Landobasa and M.K. Chin, "Phase engineering for ring enhanced Mach-Zehnder interferometers," *Optics Express,* vol. 13, no. 12, pp. 4580-4588, 2005.

[29] V. Van, "Synthesis of elliptic optical filters using mutually coupled microring resonators," *J. Lightw. Technol.,* vol. 25, no. 2, pp. 584-590, 2007.

[30] M. Sumetsky, "Vertically-stacked multi-ring resonator," *Optics Express,* vol. 13, no. 17, pp. 6354-6375, 2005.

[31] M. Sumetsky, "Uniform coil optical resonator and waveguide: transmission spectrum, eigenmodes and dispersion relation," *Optics Express,* vol. 13, no. 11, pp. 4331-4340, 2005.

[32] J. Niehusmann, et al., "Ultrahigh-quality-factor silicon-on-insulator microring resonator," *Optics Lett.,* vol. 29, no. 24, pp. 2861-2863, 2004.

[33] I. Kiyat, A. Aydinli, and N. Dagli, "High-Q silicon-on-insulator optical rib waveguide racetrack resonators," *Optics Express,* vol. 13, no. 6, pp. 1900-1905, 2005